Three-Dimensional Structure of RK-1: A Novel α-Defensin Peptide†

Ailsa M. McManus,§ Nicola F. Dawson,‡ John D. Wade,‡ Lyle E. Carrington,|| Don J. Winzor,|| and David J. Craik*,§

Centre for Drug Design and Development, Institute for Molecular Bioscience and Department of Biochemistry, University of Queensland, Brisbane, Queensland 4072, Australia, and Howard Florey Institute of Experimental Physiology and Medicine, University of Melbourne, Parkville, Victoria 3052, Australia

Received February 29, 2000; Revised Manuscript Received September 21, 2000

ABSTRACT: NMR spectroscopy and simulated annealing calculations have been used to determine the three-dimensional structure of RK-1, an antimicrobial peptide from rabbit kidney recently discovered from homology screening based on the distinctive physicochemical properties of the corticostatins/defensins. RK-1 consists of 32 residues, including six cysteines arranged into three disulfide bonds. It exhibits antimicrobial activity against *Escherichia coli* and activates Ca^{2+} channels in vitro. Through its physicochemical similarity, identical cysteine spacing, and linkage to the corticostatins/defensins, it was presumed to be a member of this family. However, RK-1 lacks both a large number of arginines in the primary sequence and a high overall positive charge, which are characteristic of this family of peptides. The three-dimensional solution structure, determined by NMR, consists of a triple-stranded antiparallel β-sheet and a series of turns and is similar to the known structures of other α-defensins. This has enabled the definitive classification of RK-1 as a member of this family of antimicrobial peptides. Ultracentrifuge measurements confirmed that like rabbit neutrophil defensins, RK-1 is monomeric in solution, in contrast to human neutrophil defensins, which are dimeric.

The vertebrate defensins are a family of highly basic, arginine-rich peptides consisting of 29−42 residues, including six disulfide-linked cysteines. Of the two subclasses within this family, the α-defensins consist of 29−35 residues, while the β-defensins are slightly longer with 38−42 residues. Both contain six disulfide-linked cysteines but differ in the position and linkage of the cysteines (*1*). Unlike many other antimicrobial peptides, the α- and β-defensins do not contain helical elements of secondary structure. They possess similar folds to each other, with a triple-stranded antiparallel β-sheet being the dominant feature. The vertebrate defensins exhibit broad-range antimicrobial activity against Gram-negative and Gram-positive bacteria, fungi, mycobacteria, spirochetes, and enveloped viruses (*2*). In addition, some members of the α-defensin family are chemotactic for monocytes at 10^{-10} M concentration (*3*), cytostatic for HL-60 promyelocyte-like cells at 10^{-9} M concentration (*4*), and some are specific antagonists of adrenocorticotropin (*5*). This latter activity has led to the α-defensin family being known as the corticostatin/defensin (CS/defs)[1] family.

The expression of genes for the α-defensins occurs in the myeloid cells as well as in the Paneth's cells of the crypt, in the intestine (*5*), confirming the existence of at least two subclasses of the CS/defs family, known as the myeloid and enteric CS/defs. The isolation of a tissue-specific defensin from intestine suggested that other such peptides might also exist and, in a recent screening study, a kidney specific defensin was isolated and characterized (*5*). This peptide, subsequently named RK-1, was found to have the same placement of cysteines and disulfide linkages as members of the α-defensin subclass (*5*, *6*). RK-1 consists of 32 residues, including the obligatory six disulfide-linked cysteines. The primary sequence, incorporating the disulfide connectivity $Cys^{I}-Cys^{VI}$, $Cys^{II}-Cys^{IV}$, and $Cys^{III}-Cys^{V}$ (*6*) is shown in Figure 1. It should also be noted that since the discovery of RK-1, a second rabbit kidney defensin, named RK-2, has been isolated and characterized (*7*).

The amino acid sequence of RK-1, unlike other members of the α-defensin family, is not arginine-rich, possessing only one such residue. Instead, the cationic character of RK-1 results from a large proportion of lysines within the primary sequence. RK-1 also contains four negatively charged residues and, at pH 7, it carries a net charge of +1, significantly lower than most other members of the α-defensin family (*5*). Finally, the sequence homology between

† The structural work was supported by a University of Queensland Travelling Scholarship (A.M.M.). Work carried out at the Howard Florey Institute was supported by an Institute Block Grant (Reg Key 983001) from the National Health and Medical Research Council of Australia.

* To whom correspondence should be addressed. Professor David J. Craik, Institute for Molecular Bioscience, University of Queensland, Brisbane, QLD 4072, Australia. Telephone: +61-7-3365-4944; fax: +61-7-3365-2487; e-mail: d.craik@mailbox.uq.edu.au.

§ Institute for Molecular Bioscience, University of Queensland.

|| Department of Biochemistry, University of Queensland.

‡ University of Melbourne.

[1] Abbreviations TOCSY, total correlation spectroscopy; NOE, nuclear Overhauser effect; NOESY, NOE spectroscopy; DQF-COSY, double-quantum filtered correlation spectroscopy; E-COSY, exclusive correlation spectroscopy; CS/defs, corticostatin/defensin; HPLC, high-pressure liquid chromatography; LUV, large unilamellar vesicles; POPG, 1-palmitoyl-2-oleoyl phosphatidylglycerol.

10.1021/bi000457l CCC: $19.00
Published on Web 11/22/2000

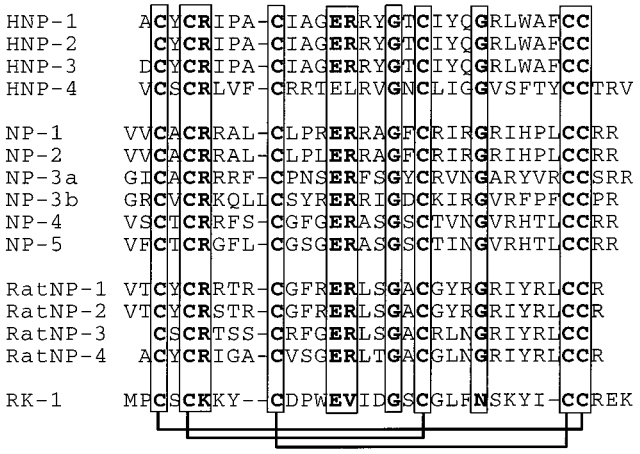

FIGURE 1: Alignment of some α-defensin sequences from human (HNP1−4), rabbit (NP1−5) and rat neutrophils (RatNP1−4) with RK-1. The lines joining pairs of cysteine residues indicate the disulfide connectivity. Conserved residues are boxed in bold.

RK-1 and the other CS-defs is low (Figure 1), suggesting that RK-1 may be the first member of a new subclass of the CS/defs (*5*).

RK-1 has antimicrobial activity against *Escherichia coli*, a common pathogen in both kidney and urinary tract infections, and it activates Ca^{2+} ion channels in vitro (*5*), an observation that has also been made for other members of this family (*5*). This activation of Ca^{2+} ion channels suggests that a second role for RK-1 in the kidney might be as a local regulator of these channels (*5*). The size and antimicrobial nature of this peptide, the placement of the cysteines in the primary sequence and the disulfide connectivity, all suggest that RK-1 is a member of the α-defensin family. However, until now the three-dimensional structure, which would resolve its membership, remained unknown. The aim of the present study was to determine the three-dimensional structure of RK-1 by nuclear magnetic resonance spectroscopy and subsequent simulated annealing structure calculations and to compare this structure to the known structures of other α-defensins.

EXPERIMENTAL PROCEDURES

Materials. RK-1 was chemically synthesized as described earlier (*6*). Samples prepared for NMR spectroscopy contained ∼1.5 mM of the peptide dissolved in the following solvent systems: 90% H_2O/10% D_2O, 100% D_2O, and 70% H_2O/3O% CD_3CN at pH 3.5.

Sedimentation Equilibrium. A solution (∼1.5 mM) of RK-1 in 90% H_2O/10% D_2O (pH 3.5) was centrifuged at 40 000 rpm and 293 K in a Beckman XL-I analytical ultracentrifuge. The resulting equilibrium distribution was recorded interferometrically and analyzed for conformity with the sedimentation expression for a single solute, namely,

$$[J(r) - J(r_m)] = J(r_m)[e^{[M\phi(r^2 - r_m^2)]} - 1]$$

$$\phi = \frac{(1 - \bar{v}\rho)\omega^2}{2RT} \quad (1)$$

to obtain best-fit values of $J(r_m)$, the concentration (in terms of interference fringes) at the air−liquid meniscus (r_m) and the reduced molecular mass ($M\phi$) from the dependence of Rayleigh fringe number, $J(r) - J(r_m)$, upon radial distance, r. Combination of the magnitude of the latter parameter with the angular velocity (ω), universal gas constant (R), and absolute temperature (T) yielded the buoyant molecular mass, $M(1 - \bar{v}\rho)$, where $\bar{v}$ is the partial specific volume of the solute and ρ is the solvent density.

NMR Spectroscopy. NMR spectra were recorded on Bruker DMX 750 MHz and Bruker ARX 500 MHz spectrometers using a 90% H_2O/10% D_2O solution of RK-1 at pH 3.5 and temperatures of 283, 298, and 308 K, a 30% CD_3CN/70% H_2O solution at 308 K, and a 100% D_2O solution at 308 K, pH 3.5. Two-dimensional homonuclear spectra were recorded in phase-sensitive mode using time proportional phase incrementation for quadrature detection in the f_1-dimension (*8*). 2D experiments included TOCSY (*9*) using an MLEV-17 spin-lock sequence (*10*) with a mixing time of 80 ms, NOESY (*11*) with mixing times of 100, 250, and 300 ms, and DQF-COSY (*12*) and E-COSY (*13*) experiments. For the DQF-COSY and E-COSY experiments, the water proton signal was suppressed by low power irradiation during the relaxation delay (1.8 s). Solvent suppression in the TOCSY and NOESY experiments was achieved using a modified WATERGATE sequence (*14*) in which two gradient pulses of 1 ms duration and 6 G cm^{-1} were applied on either side of the binomial pulse. 2D spectra were collected over 4096 data points in the f_2-dimension and 512 increments in the f_1-dimension over a spectral width corresponding to 13 ppm. TOCSY spectra were acquired with 16 scans/increment, while DQF-COSY and NOESY spectra incorporated 64 scans/increment.

Slowly exchanging NH protons were detected in a series of 1D and TOCSY spectra following the addition of D_2O to a sample of RK-1 at 308 K (pH 3.5). $^3J_{NH-\alpha H}$ coupling constants were measured from a high resolution (8 K × 1 K) DQF-COSY spectrum using line shape fitting with the program AURELIA (Bruker). $^3J_{\alpha H-\beta H}$ coupling constants were measured from a high resolution (8 K × 1 K) E-COSY spectrum.

NMR spectra were processed and analyzed on a Silicon Graphics SGI 4D/30 computer using the UXNMR software package in conjunction with X-EASY (*15*). The f_1 dimension was zero-filled to 2048 real data points with the f_1 and f_2 dimensions being multiplied by a sine-squared function shifted by 90° prior to Fourier transformation. Polynomial baseline correction was used in selected regions to improve the appearance of the spectrum. Chemical shifts were referenced to internal DSS.

Structure Calculations. Peak volumes in the 100 ms NOESY spectra (90% H_2O/10% D_2O, 308 K, 100% D_2O, 308 K) were measured in XEASY. These were classified as strong, medium, weak, or very weak corresponding to upper bounds of 2.7, 3.5, 5.0, or 6.0 Å, respectively (*16*). The upper limits of methylene, methyl, and aromatic protons were adjusted using standard pseudoatom corrections (*17*). An additional 0.5 Å was added to restraints involving methyl protons.

Backbone ϕ dihedral angle restraints were derived from $^3J_{NH-\alpha H}$ coupling constants, with ϕ restrained to −60° ± 30 for $^3J_{NH-\alpha H}$ = <5.8 Hz (residues K7, F22, S24), −120° ± 30 for $^3J_{NH-\alpha H}$ = 8.0−9.5 Hz (residues C3, K6, C9, D10, W12, E13, V14, D16, S18, L21, K25, I27, and C28), and −120° ± 15 for $^3J_{NH-\alpha H}$ > 9.5 Hz (residues Y26, C29).

These measurements were made from line shape analysis of the antiphase cross-peak splitting in the DQF-COSY spectrum. Additional dihedral angle restraints of $-100° \pm 80$ were added where it was clear the intraresidual $\alpha_i \rightarrow NH_i$ NOE was weaker than the $\alpha_{i-1} \rightarrow NH_i$ NOE (residues I15, R30, E31, K32). Restraints of and $50° \pm 40$ were also added when an intense intraresidual H_α-H_N NOE was measured along with a $^3J_{NH-\alpha H} \sim 7$ Hz (residue N23) (*18*). χ^1 restraints were added for a number of side chains on the basis of observed NOEs and $^3J_{\alpha H-\beta H}$ coupling constants (*19*). g^2g^3 and t^2g^3 conformations were restrained to $60° \pm 30$ (I15, C19, and L21) and $-60° \pm 30$ (K6, C9, D10, and Y26), respectively.

Three-dimensional structures were calculated using simulated annealing and energy minimization protocols within X-PLOR (*20*). An ab initio simulated annealing protocol incorporating ambiguous distance restraints and floating point chirality was used to generate a set of 50 structures starting from a template structure with randomized φ and ϕ angles and extended side chains (*21*, *22*). This protocol consisted of 50 ps of molecular dynamics at 2000 K followed by 15 ps of cooling to 100 K. The 50 calculated structures were then subjected to 2000 cycles of energy minimization using the conjugate gradient Powell algorithm under the influence of the CHARMm force field (*23*, *24*). Electrostatic terms involving side chain/side chain interactions were excluded from the energy function during refinement so as not to place undue emphasis on charge−charge interactions in the absence of solvent molecules in the calculations. Standard XPLOR parameters were used for electrostatic terms involving backbone atoms (parameter file: h3x2.pro) (*20*).

Disulfide bonds with the connectivity Cys3−Cys29, Cys5−Cys19, and Cys9−Cys28, determined in a previous study (*6*), were incorporated into the structure calculations using standard XPLOR geometries and force constants (parameter and topology file, parallhdg.pro and topallhdg.pro (*20*), respectively). In an attempt to understand the origin of one of the minor conformers (see Results), an additional set of structures was calculated in which the Cys3−Cys29 disulfide bond was constrained to either −90° or 90°.

The coordinates for the 20 refined, lowest energy conformers have been deposited in the Protein Data Bank under the accession code 1EWS.

RESULTS

RK-1 was chemically synthesized as described previously (*6*) and purified as a single isomer in good yield and high purity. Because of the tendency of defensins to form dimers (*25*, *26*), the macromolecular state of the peptide was assessed by sedimentation equilibrium studies under conditions (90% H_2O/10% D_2O, pH 3.5, 293 K) pertinent to those used for structure determination by NMR. Despite a gradual loss of solute as the result of precipitation during the early stages of the experiment, the Rayleigh fringe pattern had attained the time-independence characteristic of sedimentation equilibrium attainment after 24 h. Nonlinear regression analysis of the dependence of Rayleigh fringe number upon radial distance (Figure 2) in terms of eq 1 signified best-fit values (± 2SD) of 1.62 (± 0.002) for the meniscus concentration and the product $M\phi$, respectively. On the basis of the partial specific volume of 0.72 mL/g that is calculated from the amino acid composition, the value of $M\phi$ translates into an apparent molecular mass of 4200 (± 40) Da for the single sedimenting species. The slight disparity between this estimate and the calculated molecular mass of 3700 Da is almost certainly attributable to one or both of two factors. (i) The magnitude calculated for $\bar{v}$ takes no account of the contribution by proton and hydroxyl counterions that form part of the sedimenting species in a medium devoid of supporting electrolyte. (ii) Discrepancies of this order of magnitude are likely to arise in the estimate of M by two parameter curve-fitting to eq 1 (*27*). We therefore conclude that RK-1 is monomeric in the environment to be used for determining the three-dimensional structure of the peptide.

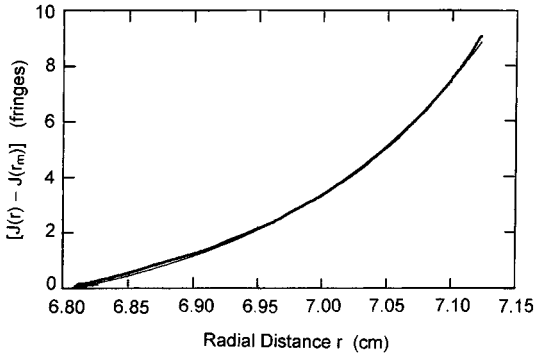

FIGURE 2: Analysis of a sedimentation equilibrium distribution for RK-1 in 90% H_2O/10% D_2O (40 000 rpm, 293 K) by direct curve-fitting of the Rayleigh interference data to eq 1 to obtain $J(r_m)$ as well as the buoyant molecular mass: the thin line is the best-fit description obtained by nonlinear regression analysis.

Spectral Assignments. Peak assignments (Supporting Information) were made from DQF-COSY, TOCSY, and NOESY spectra acquired on the peptide at 308 K in 90% H_2O/10% D_2O, and from E-COSY and NOESY spectra acquired in 100% D_2O. Some supplementary spectra in 30% CD_3CN/70% H_2O were acquired to ensure that no structural change was observed with more hydrophobic solution conditions. These spectra were helpful in resolving a few ambiguities, but the NOE data used for deriving structural information were primarily obtained from spectra recorded in aqueous solution.

From an analysis of the 750 MHz spectra, it was obvious that more spin systems were present than would be expected for a single isomer or conformer of a 32-residue peptide. Through the sequential and long-range assignment of peaks in the NOESY spectrum, it became clear the single isomer of RK-1, isolated by HPLC, exists in solution in three conformations. The major one (conformer 1) accounts for ∼85% of the peak intensity with the other two having relative intensities of ∼5% (conformer 2) and ∼10% (conformer 3). For residues 3−6, 12−14, and 29−30, three spin systems were observed, whereas for residues 1−2, 8, 10, and 31−32, two spin systems were assigned. Almost complete assignments were made for the three conformers, although the chemical shifts of two, or sometimes all three conformers, were degenerate for many residues. An analysis of αH and NH chemical shifts (Supporting Information) showed that conformer 2 is most similar to conformer 1, with αH shifts differing by less than 0.1 ppm in most cases. In contrast, conformer 3 is more different over certain residues, particularly 3−7, 9−14, and 29−31.

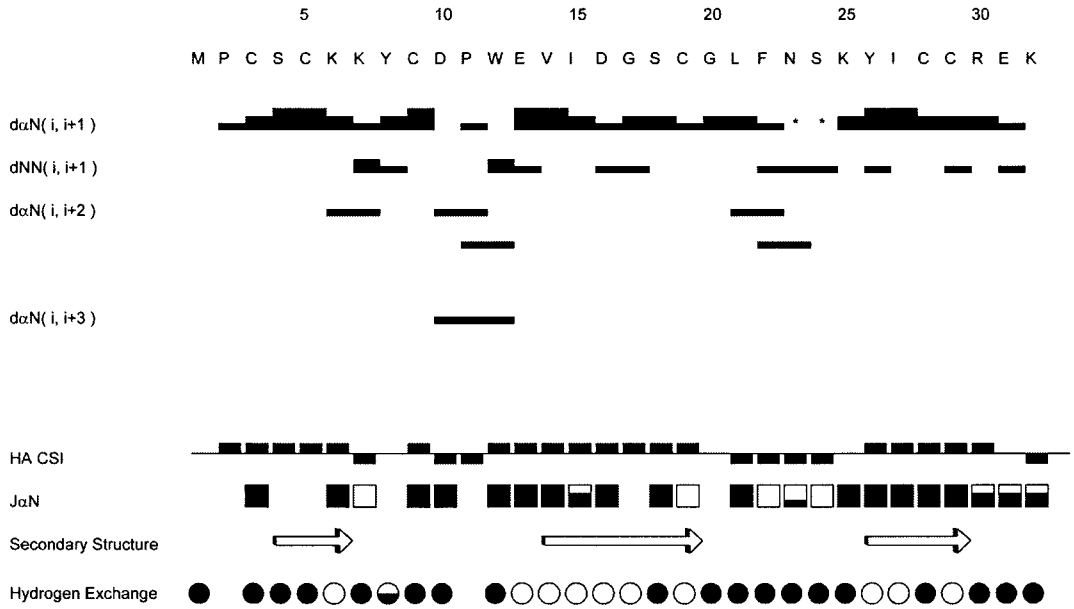

FIGURE 3: Summary of NOE connectivities for RK-1. The intensity of NOEs is indicated by the thickness of the line, grouped into strong, medium, and weak. An asterisk indicates overlapping, and therefore ambiguous, cross-peaks. Empty circles represent slowly exchanging amides still present after 12 h. Half-filled circles represent medium-exchanging amides still present after 5 h. Large (>9.5 Hz) and small (<5 Hz) $^3J_{\alpha H-NH}$ coupling constants are represented by black and white squares, respectively. Arrows represent the regions of β-strands found in RK-1.

Since cis/trans isomerization of X-Pro bonds is often the cause of conformational heterogeneity, the NOE data associated with the two proline residues in RK-1 were examined. In the case of Pro11, a $d\alpha_{i-1\rightarrow}\delta_i$ NOE between the Pro and the preceding Asp residue confirmed the trans nature of the intervening peptide bond in the major conformation. It was not possible to unambiguously determine the cis/trans nature of this bond in the two minor conformers. In contrast, the observation of a strong $d\alpha_{i-1\rightarrow}\delta_i$ NOE between Met1 and Pro2 in conformer 1, and a corresponding strong $d\alpha_{i-1\rightarrow}\alpha_i$ NOE between Met1 and Pro2 in conformer 3, suggests that this bond is trans in conformer 1 and cis in conformer 3. This is consistent with a heterogeneity of peaks associated with residues near Pro2.

Secondary Structure. The short- and medium-range NOEs, chemical shift indices, NH exchange rates, and $^3J_{NH-\alpha H}$ coupling constants, observed for the major conformer of RK-1, are summarized in Figure 3. From this information and the assignment of long-range NOEs, it was possible to identify the secondary structure, shown in Figure 4, as consisting of an antiparallel β-sheet made of three β-strands, including a β-hairpin. The extent of the β-sheet structure is particularly well-emphasized by the slow exchange data. 12 h after dissolution in D_2O, 10 of the 30 backbone NH groups had not exchanged. An additional NH group remained visible in spectra for 5 h after dissolution in D_2O. The great majority of these slowly exchanging amides (Figure 3) are in the β-strand regions of the peptide and indicate hydrogen bonding across the sheets. In addition, most coupling constants measured from the DQF-COSY spectrum are >8.0 Hz (Figure 3), which is consistent with the extensive β-sheet secondary structure of RK-1. This conclusion is strongly supported by the CSI data, which show three contiguous stretches of positive CSI values over residues 2−6, 12−19, and 26−30.

RK-1 contains six disulfide-linked cysteines. In a recent study (*6*), the disulfide connectivity was deduced from an analysis of NOEs between the cysteines, since it was not possible to determine the cysteine linkage by chemical methods. That study concluded that the disulfide connectivity was $Cys^{I} \rightarrow Cys^{VI}$, $Cys^{II} \rightarrow Cys^{IV}$, and $Cys^{III} \rightarrow Cys^{V}$, as is found in the other α-defensins. In the current study, this connectivity was definitively confirmed using the complete ensemble of NOEs in three-dimensional structure calculations.

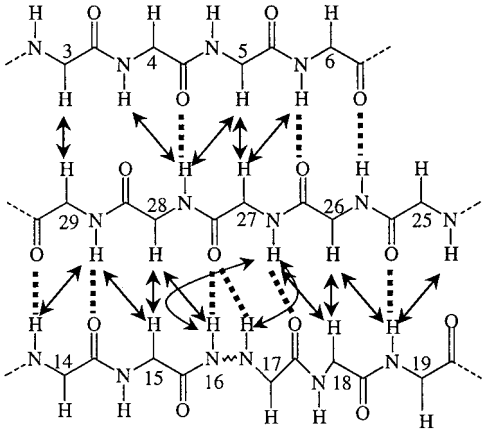

FIGURE 4: Schematic diagram of the sheet regions of RK-1. Arrows represent the observation of NOEs between protons. Dashed lines represent hydrogen bonds deduced on the basis of slow-exchanging amide protons.

Three-Dimensional Structure Determination. NOESY spectra were used to derive a set of 509 distance restraints consisting of 244 intraresidual, 110 sequential, 25 medium-range, 119 long-range distance restraints, and 11 H-bond restraints for the main conformer of RK-1. An additional 31 dihedral angle restraints were obtained from the DQF-COSY and E-COSY spectra and, together with the distance restraints, were used to calculate a set of 50 structures.

On the basis of lowest energies, 20 structures, from the calculated set of 50, were selected to represent the solution

Table 1: Structural and Energetic Statistics for a Family of 20 RK-1 Structures

mean RMSD from exp distance restraints	
NOE (Å)	0.009 ± 0.001
dihedral (°)	0.29 ± 0.06
mean RSMD from idealized covalent geometry	
bonds (Å)	0.0072 ± 0.0003
angles (°)	2.04 ± 0.02
impropers (°)	0.14 ± 0.02
restraint violations	
NOE violations > 0.1 Å	0.35 ± 0.06
maximum violation (Å)	0.141
dihedral angle violations > 1°	1.05 ± 0.69
maximum violation (°)	2.1
pairwise RMSD[a]	
backbone atoms 1−32 (N, Cα, C) (Å)	1.41 ± 0.34 (1.57 ± 0.42)
heavy atoms (Å)	2.59 ± 0.31 (2.73 ± 0.49)
backbone atoms 3−29 (N, Cα, C) (Å)	0.56 ± 0.13 (0.62 ± 0.16)
heavy atoms (Å)	1.62 ± 0.28 (1.71 ± 0.31)
Ramachandran plot	
residues in most favored regions	61.4%
residues in additional allowed regions	36.1%
residues in generously allowed regions	2.6%
residues in disallowed regions	0.0%

[a] Forty-three of 509 restraints were derived from the 30% CD_3CN/70% H_2O data. The data shown in parentheses were derived from structures calculated without these restraints and confirm that the structures calculated using data recorded in water alone yield essentially identical structures to those recorded in 30% CD_3CN/70% H_2O.

structure of RK-1. The 20 selected structures all have NOE violations less than 0.15 Å and dihedral violations less than 1.5°. The statistical data summarizing the quality of these 20 structures are presented in Table 1. As is evident from the backbone overlay shown in Figure 5, these structures are precisely defined. The average pairwise RMSDs for the backbone atoms (N, C, C_α) and heavy atoms over residues 3−29 are 0.56 and 1.62 Å, respectively (Table 1). In addition, 100% of the backbone angles in the 20 structures fall into the allowed regions of the Ramachandran plot (Table 1) (*28*).

The major structural elements of RK-1 (Figure 6) are three β-strands, including a β-hairpin, arranged into one antiparallel β-sheet. The three strands encompass residues 4−6, 14−18, and 26−29, and incorporate a classic β-bulge (*29*) involving residues Asp16, Gly17, and Ile27. The strands of RK-1 are linked by a series of tight turns. A type I turn (*29*, *30*) is present at residues 10−13, a type IV turn at residues 6−9 and a composite turn at residues 20−24. This composite turn includes an inverse γ-turn between Leu21 and Asn23. The conformations of the disulfide bonds Cys5−Cys19 and Cys9−Cys28 are a right-handed spiral and a right-handed hook, respectively (*29*), while the Cys3−Cys29 disulfide bond occupies both right-handed and left-handed conformations among the ensemble of structures. The disulfide bonds link the two ends of the molecule, the first β-strand to the loop between the second and third β-strand, and the loop between the first and second β-strands to the third β-strand.

These structural findings apply to the major (85%) conformation in solution; however, two other conformers were also detected. The one that is most different from the major isomer, conformer 3, can readily be explained by a cis imide bond at Pro2. The origin of conformer 2 was less clear from an inspection of the NOE and chemical shift data alone. Its NH and αH shifts differ only slightly from the main conformer and hence is likely to be similar in structure. On the basis of the calculated structure for the major conformer, one possibility considered was that the Cys3−Cys29 disulfide bond might exist in both the Pro-R and Pro-S conformations. It seemed unlikely that either Cys5−Cys19 or Cys9−Cys28 linkages were involved in such isomerization, as the coupling constant data clearly indicated that the χ^1 angles of Cys9 and Cys19 are constrained. In addition, analysis of the final structures showed that these disulfide linkages are largely in the one conformation, whereas for the Cys3−Cys29 bond, there is an equal distribution of right- and left-handed disulfide bond combinations. Also, the duplication αH and NH peaks is greatest at the two ends of the molecule, in proximity with the Cys3−Cys29 disulfide linkage. The ProR−ProS hypothesis was tested through the calculation of two sets of structures, each with the Cys3−Cys29 disulfide bond restrained to either −90° or 90°. Analysis of these structures suggested that the Pro-R/Pro-S isomerization only affects the local structure slightly and confirmed this as the likely origin of conformer 2.

DISCUSSION

The aim of this study was to determine the three-dimensional structure of RK-1, a novel antimicrobial peptide isolated from rabbit kidney, with a view to definitively classify it as a member, or otherwise, of the α-defensin family. The results conclusively show the three-dimensional structure of RK-1 is similar to the other α-defensins, and therefore, this peptide can be defined as a new member of the family. The three-dimensional structure consists of three β-strands, including a β-hairpin, which align to form an antiparallel β-sheet. The strands of the sheet are joined to each other by a series of tight turns. The type, number, and positions of the β-strands are similar to those in other α-defensins (*25*, *26*), and the disulfide connectivity is identical to other α-defensins. In addition, RK-1 contains a classic β-bulge that is homologous to one containing a conserved glycine at position 17 or 18 in HNP-1, HNP-3, and NP-2 (*26*).

Two minor conformers were also detected: one associated with cis/trans isomerization at Pro2 and the other most likely due to ProR/ProS isomerization of the Cys3−Cys29 disulfide bond. The biological significance of these minor forms is not known and will be difficult to ascertain because they are not separable. RK-1 elutes as a single peak on HPLC, and the minor conformers only become apparent in NMR solution studies. However, since they appear to be so similar to the major form, it is unlikely that they differ significantly in their mode of action. The remainder of the discussion focuses on the major conformer.

The only published coordinates for another α-defensin are from an X-ray study on HNP-3, which forms a dimeric structure (*28*). From Figure 7, it is clear that the solution structure of RK-1 overlays well with the monomer unit from this structure (pdb code: 1dfn) (*25*), confirming their similar three-dimensional topologies. There are, however, some differences between the structures. First, there is a type II turn encompassing residues 11−14 in HNP-3, whereas in RK-1, the turn encompassing the corresponding residues, 10−13, is type I. Second, there is a difference in the orientation of the β-hairpin loop between strands 2 and 3 of the β-sheet. In HNP-3, residues 21−25 form a composite turn comprising type IV and I′ turns. RK-1 also possess a

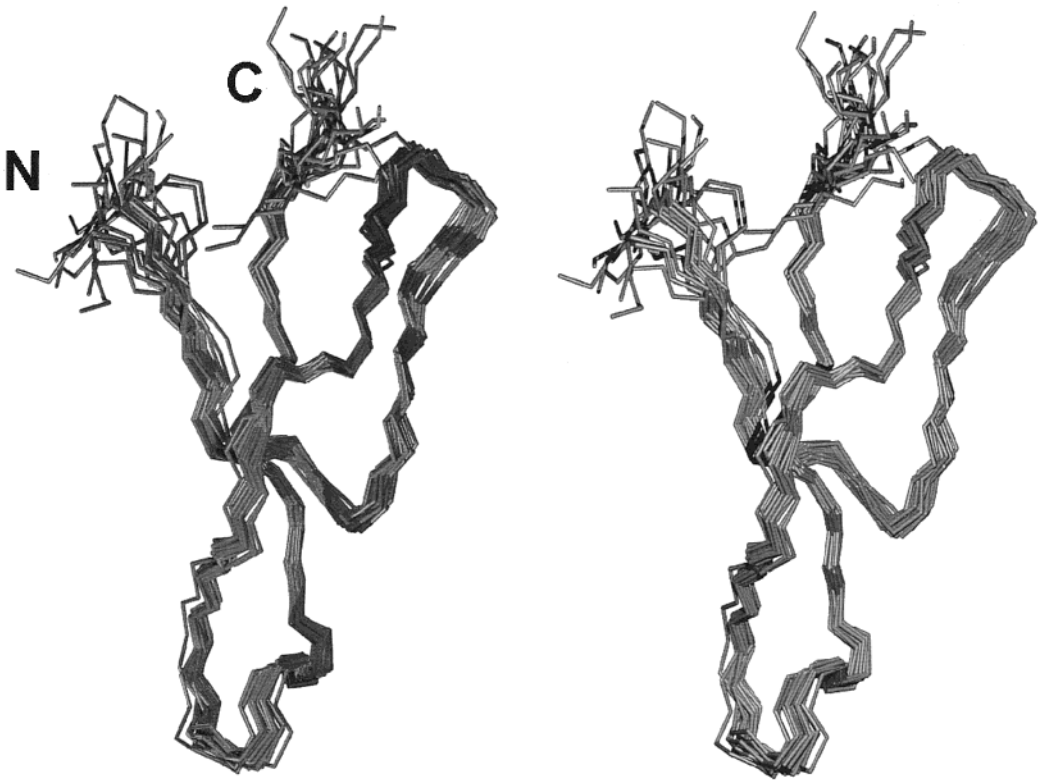

FIGURE 5: Stereoview of the backbone superimposition of the 20 lowest energy structures of RK-1. The figure was prepared using the program MOLMOL (*36*).

FIGURE 6: One of the 20 lowest energy structures of RK-1. The β-strands are represented with arrows and disulfide bonds are shown in ball-and-stick representation. The figure was prepared using the program MOLMOL (*36*).

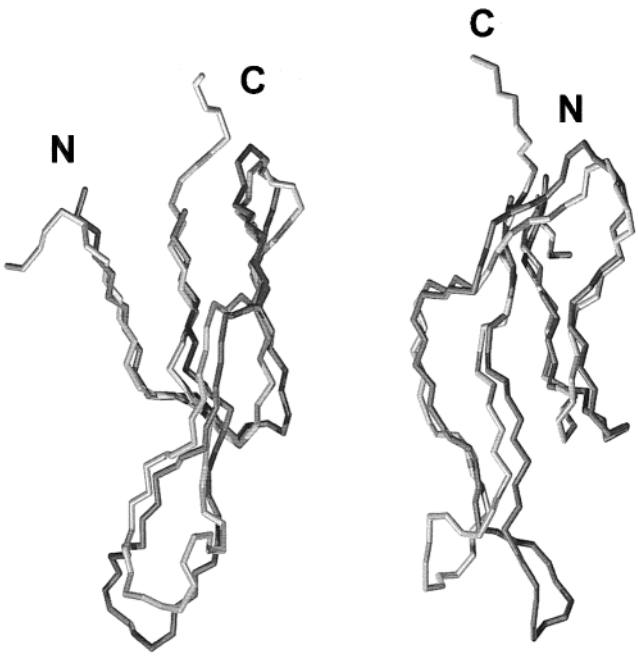

FIGURE 7: Two views of an overlay of the crystal structure of HNP-3 (PDB ID code: 1dfn) (dark gray) and the solution NMR structure of RK-1 (light gray). HNP-3 exists as a dimer in the crystal structure and only one of the monomers is shown.

composite turn in this region, comprising an inverse γ-turn and two type IV turns; however, the orientation at the end of the hairpin differs (Figure 7). This structural difference in the β-hairpin is particularly interesting given the results of a recent study that suggested that the β-hairpin loop of the rabbit neutrophil defensin, NP-2, was the active part of the molecule (*31*). Indeed, the β-hairpin loop is conserved throughout all the mammalian, insect, and plant defensins that have been characterized to date (*31*).

A number of studies have investigated the structure−activity relationships of members of the α-defensin family (*1*, *25*, *26*, *31*−*33*). In all cases, it has been shown that the defensins possess amphipathic structures and cause permeabilization of the cell membranes of a broad-range of microbes (*32*). It would appear, however, that the mode of permeabilization differs between human and rabbit neutrophil defensins. It is believed this difference in mode of action is

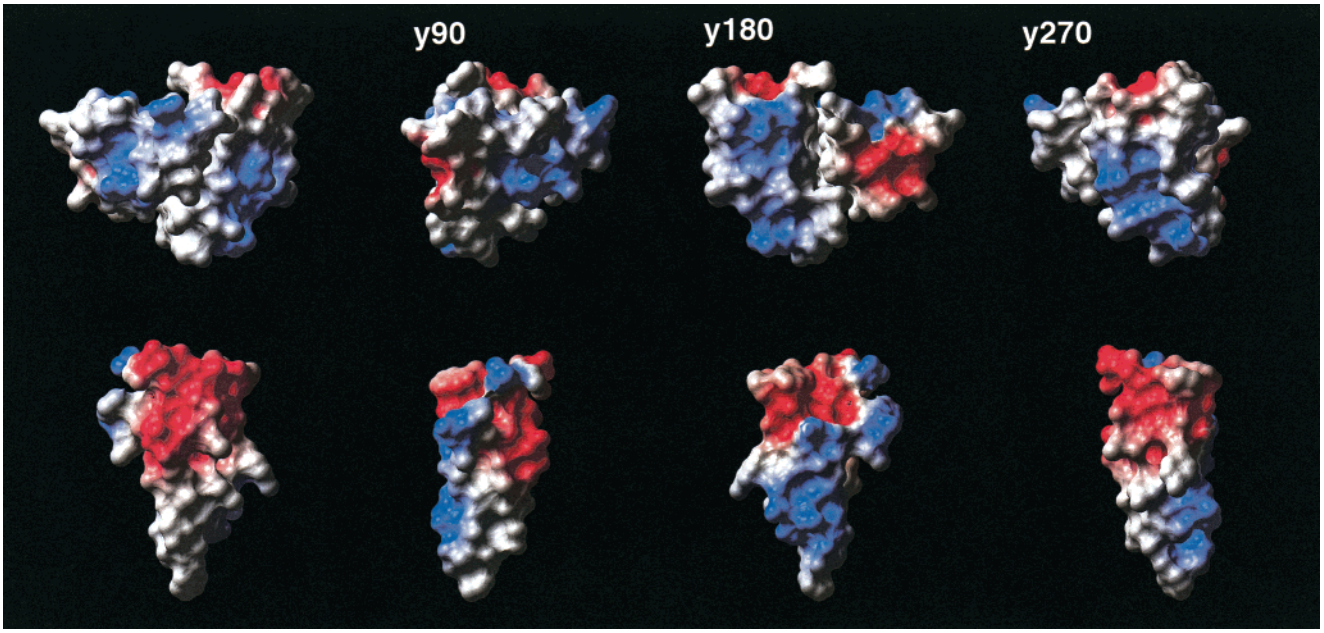

FIGURE 8: Electrostatic surface potentials of the HNP-3 dimer (top) and RK-1 (bottom). Successive structures are rotated by 90° around the vertical axis. RK-1 has a very distinct separation of positive and negative charge with the negative charge being contained within the top half of the molecule and the positive charge mostly within the bottom half. In addition, RK-1 has a small uncharged surface located on the bottom half of the molecule.

related to the fact human neutrophil defensins form stable dimers whereas the rabbit neutrophil defensins exist in a monomeric state (*26*, *33*).

In the case of the human neutrophil defensin, HNP-2, permeabilization of large unilamellar vesicles (LUVs) made from pure 1-palmitoyl-2-oleoyl phosphatidylglycerol (POPG) bilayers occurs when the peptides aggregate to form large, long-lived multimeric pores (*32*). A model for this pore that is made up of six HNP-2 dimers has been proposed (*34*). In contrast, the rabbit neutrophil defensins, NP-1, NP-2, NP-3a, NP-3b, and NP-5, appear not to form long-lived pores but interact in a way that causes only a graded leakage of the cell contents from POPG LUV (*33*). NP-4 had no effect on the model membrane. In LUVs made from lipid extracts of *E. coli* membranes, the rabbit defensins NP-1, NP-2, NP-3a, and NP-3b caused transient pores in the membrane. While neither NP-4 or NP-5 had any direct effect, they did have a synergistic effect on the activity of NP-1, NP-2, NP-3a, and NP-3b (*32*). It was hypothesized that the reason NP-4 and NP-5 were unable to permeabilize the membrane was a result of their low overall positive charge and/or the lack of a charged residue at position 21 in the primary sequence (*32*). It was noted that NP-1, NP-2, NP-3a, and NP3b all have either lysine or arginine at this position, whereas both NP-4 and NP-5 have a threonine at this position. Interestingly, the human neutrophil defensins have either an isoleucine or leucine at this position, which is situated at the monomer−monomer interface, and it was speculated (*32*) that this may be important for dimerization of these defensins.

RK-1 is believed to form a new subclass of the α-defensins resulting from gene duplication and subsequent evolution (*7*). While RK-1 does have homology to the other α-defensins (Figure 1), it possesses a significantly lower overall charge than other family members. As has already been noted, the human neutrophil defensins form dimers, whereas the rabbit neutrophil defensins exist as monomers. Since RK-1 forms a new subclass, there was interest in determining whether RK-1 existed as a monomer or a dimer in solution, particularly since past studies had indicated a difference in the modes of actions of the rabbit and human neutrophil defensins (*32*, *33*). In a previous study, it was noted that the human neutrophil defensin (HNP-1) had a large number of slow-exchanging amide protons that could only be reconciled with the presence of a dimer or higher-order aggregate (*1*, *26*, *35*). However, in the current study of RK-1, the number of slowly exchanging amide protons was consistent with the sole presence of a monomer species, and there was no other NMR evidence suggesting a dimeric state. In addition, ultracentrifuge measurements showed that under the NMR conditions RK-1 was a monomer. Thus, the current study clearly established that RK-1 exists as a monomer in solution.

The surface representation in Figure 8 shows that RK-1 has a conical shape with partial amphipathic character in that most hydrophobic residues are co-located near the apex end of the cone (lower part of Figure 8). More striking is the clear separation of positive and negative charges in RK-1. The HNP-3 dimer is shown for comparison, with one of the monomer units in a similar orientation to the monomer of RK-1. The higher surface exposure of positive charges in HNP-3 relative to RK-1 is apparent from this comparison. Individual monomers of HNP-3 (not shown) have a much larger uncharged surface area than RK-1. This uncharged region is mostly buried in the dimer, and it is believed that one of the driving forces for the formation of the dimer is associated with these hydrophobic interactions (*25*). RK-1 lacks this large uncharged region, most likely explaining why RK-1 does not form a dimer.

Since RK-1 appears to be a monomer, it seems likely that it acts similarly to the rabbit neutrophil defensins, causing the formation of transient rather than long-lived pores in the membrane of *E. coli*. It was hypothesized by Hristova et al. (*32*) that the low overall charge of NP-4 and NP-5 perhaps prevented their permeabilization of the membrane. RK-1 also has a low overall charge, but it does have antimicrobial

activity against *E. coli* (*5*), so low charge is not necessarily correlated with lack of membrane permeabilization. Hristova et al. (*32*) alternatively hypothesized that the presence of an arginine or lysine at position 21, which is the residue following the fourth cysteine, may be essential for membrane permeabilization. Again, however, RK-1 is active against *E. coli* and has a glycine rather than lysine or arginine at this position. Thus, the new data for RK-1 show that further work is necessary before a full understanding of the mechanisms of action of these antimicrobial peptides will be obtained.

In summary, this study has proven conclusively that RK-1 is a bona fide member of the corticostatin/defensin class of antimicrobial peptides. The structure of RK-1 has also provided preliminary insights into structure−activity relationships of this peptide. RK-1 appears to be a monomer, and therefore, its mode of action may be similar to the rabbit neutrophil defensins that are thought to form transient pores in the *E. coli* membrane (*32*). Future work will concentrate on more clearly defining structure−activity relationships of RK-1 through the design, expression, and analysis of mutants.

ACKNOWLEDGMENT

D.J.C. is an Australian Research Council Senior Fellow. The Institute for Molecular Bioscience is a Special Research Centre of the Australian Research Council.

SUPPORTING INFORMATION AVAILABLE

Fingerprint region of the NOESY spectrum of RK-1 showing the relative positions of the NH and αH chemical shifts (Figure S1). Chemical shift differences between conformer 1 and conformers 2 and 3 (Figure S2). ^{1}H NMR chemical shifts of RK-1 in 90% H_2O/10% D_2O at 308 K (Table 1). This material is available free of charge via the Internet at http://pubs.acs.org.

REFERENCES

1. White, S. H., Wimley, W. C., and Selsted, M. E. (1995) *Curr. Opin. Struct. Biol. 5*, 521.
2. Nicolas, P., and Mor, A. (1995) *Annu. Rev. Microbiol. 49*, 277.
3. Territo, M. C., Ganz, T., Selsted, M. E., and Lehrer, R. (1989) *J. Clin. Invest. 84*, 2017.
4. Bateman, A., Singh, A., Fernando Congote, L., and Solomon, S. (1991) *Regul. Pept. 35*, 135.
5. Bateman, A., MacLeod, R. J., Lembessis, P., Hu, J., Esch, F., and Solomon, S. (1996) *J. Biol. Chem. 271*, 10654.
6. Dawson, N. F., Craik, D. J., McManus, A. M., Dashper, S. G., Reynolds, E. C., Tregear, G. W., Otvos, L., and Wade, J. D. (2000) *J. Pept. Sci. 6*, 19.
7. Wu, E.-R., Daniel, R., and Bateman, A. (1998) *Peptides 19*, 793.
8. Marion, D., and Wüthrich, K. (1983) *Biochem. Biophys. Res. Commun. 113*, 967.
9. Braünschweiler, L., and Ernst, R. R. (1983) *J. Magn. Reson. 53*, 521.
10. Bax, A., and Davis, D. G. (1985) *J. Magn. Reson. 65*, 355.
11. Jeneer, J., Meier, B. H., Bachmann, P., and Ernst, R. R. (1979) *J. Chem. Phys. 71*, 4546.
12. Rance, M., Sørenson, O. W., Bodenhausen, G., Wagner, G., Ernst, R. R., and Wüthrich, K. (1983) *Biochem. Biophys. Res. Commun. 117*, 479.
13. Greisinger, C., Sorensen, O. W., and Ernst, R. R. (1987) *J. Magn. Reson. 88*, 177.
14. Piotto, M., Saudek, V., and Sklenar, V. (1992) *J. Biomol. NMR 2*, 661.
15. Eccles, C., Güntert, P., Billeter, M., and Wüthrich, K. (1991) *J. Biomol. NMR 1*, 111.
16. Clore, G. M., Brünger, A. T., Karplus, M., and Gronenborn, A. M. (1986) *J. Mol. Biol. 191*, 523.
17. Wüthrich, K., Billeter, M., and Braun, W. (1983) *J. Mol. Biol. 169*, 949.
18. Clubb, R. T., Ferguson, S. B., Walsh, C. T., and Wagner, G. (1994) *Biochemistry 33*, 2761.
19. Wagner, G. (1990) *Prog. Nuc. Magn. Reson. Sp. 22*, 101.
20. Brünger, A. T. (1992) *X-PLOR Manual*, Version 3.1, Yale University, New Haven.
21. Nilges, M., Gronenborn, A. M., Brünger, A. T., and Clore, G. M. (1988) *Protein Eng. 2*, 27.
22. Folmer, R. H., Hilbers, C. W., Koning, R. N., and Nilges, M. (1997) *J. Biomol. NMR 9*, 245.
23. Clore, G. M., Nilges, M., Sukuraman, D. K., Brünger, A. T., Karplus, M., and Gronenborn, A. M. (1986) *EMBO J. 5*, 2729.
24. Brooks, R. R., Bruccoleri, R. E., Olafson, B. D., States, D. J., Swaminathan, S., and Karplus, M. (1983) *J. Comput. Chem. 4*, 187.
25. Hill, C. P., Yee, J., Selsted, M. E., and Eisenberg, D. (1991) *Science 251*, 1481.
26. Pardi, A., Zhang, X.-L., Selsted, M. E., Skalicky, J. J., and Yip, P. F. (1992) *Biochemistry 31*, 11357.
27. Hall, D. R., Harding, S. E., and Winzor, D. J. (1999) *Prog. Colloid Polym. Sci. 113*, 62.
28. Laskowski, R. A., MacArthur, M. W., Moss, D. S., and Thornton, J. M. (1993) *J. Appl. Crystallogr. 26*, 283.
29. Hutchinson, E. G., and Thornton, J. M. (1996) *Protein Sci. 5*, 212.
30. Lewis, P. N., Momany, F. A., and Scheraga, H. A. (1973) *Biochim. Biophys. Acta 303*, 211.
31. Thennarasu, S., and Nagaraj, R. (1999) *Biochem. Biophys. Res. Commun. 254*, 281.
32. Hristova, K., Selsted, M. E., and White, S. H. (1997) *J. Biol. Chem. 272*, 24224.
33. Hristova, K., Selsted, M. E., and White, S. H. (1996) *Biochemistry 35*, 11888.
34. Wimley, W. C., Selsted, M. E., and White, S. H. (1994) *Protein Sci. 3*, 1362.
35. Skalicky, J. J., Selsted, M. E., and Pardi, A. (1994) *Proteins 20*, 52.
36. Koradi, R., Billeter, M., and Wüthrich, K. (1996) *J. Mol. Graphics 14*, 51.

BI000457L